Available online at www.sciencedirect.com

ScienceDirect

Procedia IUTAM 14 (2015) 487 – 495

Procedia IUTAM

www.elsevier.com/locate/procedia

IUTAM_ABCM Symposium on Laminar Turbulent Transition

Heat transfer analysis in a flow over concave wall with primary and secondary instabilities

Vinicius Malatesta[a,b,c], Leandro F. Souza[b,*], Joseph T. C. Liu[c], Markus J. Kloker[d]

[a] *Mobility Engineering Center, Federal University of Santa Catarina, Joinville, Santa Catarina, Brazil*
[b] *Department of Applied Mathematics and Statistics, Institute of Mathematics and Computational Sciences, University of São Paulo, São Carlos, São Paulo, Brazil*
[c] *School of Engineering and Center for Fluid Mechanics, Brown University, Providence, Rhode Island, USA*
[d] *Institute of Aerodynamics and Gasdynamics, University of Stuttgart, Stuttgart, Germany.*

Abstract

The centrifugal instability mechanism in boundary layers over concave surfaces is responsible for the development of counter-rotating vortices, aligned in the streamwise direction, known as Görtler vortices. These vortices create two regions in the spanwise direction, the upwash and downwash regions. The downwash region is responsible for compressing the boundary layer towards the wall, increasing the drag coefficient and the heat transfer rate. The upwash region does the opposite. The Görtler vortices distort the streamwise velocity profile in the spanwise and the wall-normal directions. These distortions generate inflections in the distribution of streamwise velocity that are unstable to unsteady disturbances giving rise to secondary instabilities. In these flows the secondary instabilities can be of varicose or sinuous mode. The present paper analyses the heat transfer in a flow over a concave wall subjected to primary and secondary instabilities. The research is carried out by a Spatial Direct Numerical Simulation. The adopted parameters mimic the experimental parameters of Winoto and collaborators[17,18] and the Prandtl number adopted was $Pr = 0.72$. The results show that the varicose mode is the dominant secondary instability for the adopted parameters and that the spanwise average heat transfer rates can reach higher values than the turbulent ones. The higher heat transfer is caused by the mean flow distortion induced by the vortices, and this is present before high–frequency secondary instability sets in. Hence there is no direct connection to secondary instability. Possibly low–frequency modes undergo instability earlier.

Selection and peer-review under responsibility of ABCM (Brazilian Society of Mechanical Sciences and Engineering)

Keywords: Centrifugal instability, Secondary instability, Heat transfer, Spatial direct numerical simulation.

1. Introduction

According to Drazin[2] the hydrodynamic instability can occur due to rotation effects on concave surfaces. Examples are the Couette flow, the flow in a curved channel due to the pressure gradient acting around the curved channel, and the boundary layer over a the concave surface. This latter is the focus of this study.

* Corresponding author. Tel.: +55-16-3373-9675.
E-mail address: lefraso@icmc.usp.br

Selection and peer-review under responsibility of ABCM (Brazilian Society of Mechanical Sciences and Engineering)
doi:10.1016/j.piutam.2015.03.077

The first researcher to study the mechanism of inviscid centrifugal instability was Rayleigh[24], which derived the Rayleigh circulation criterion for instability, furthermore noted that there is an analogy between the rotational flow stability and the stability in a stratified fluid at rest in a gravitational field.

The first experimental study which showed that the curvature of the wall has a strong effect on boundary layer transition were conducted by Clauser and Clauser[1]. In their experiment it was studied the effects of concave and convex curvature on laminar-turbulent transition. Theoretical analysis was carried out for checking that a flow that is more stable on concave surfaces than convex surfaces and this was confirmed experimentally. Görtler[6] showed the existence of centrifugal instability on concave surfaces and defined a dimensionless parameter that carries his name, the Görtler number Go.

The Görtler instability is characterized to modify the streamwise velocity distribution in the longitudinal direction of flow, thus two regions are formed, upwash and downwash regions. In the upwash region the flow near the wall is thrown far away, thus the boundary layer becomes thicker. In the downwash region the opposite occurs, the higher speed flow it is compressed to the wall. In the nonlinear development region a mushroom-type structure is observed for the streamwise velocity distribution in a crosscut plane.

Swearingen and Blackwelder[32] presented experimental results where the initial boundary layer over a concave wall, quickly becomes three-dimensional. This behavior is caused by longitudinal vortices that grows in agreement with the Görtler linear analysis. In their study the mushroom-like structures were observed. The new boundary layer obtained is more complex than the initial one. This new velocity distribution can become unstable to other disturbances. These new instabilities are known as secondary instabilities, which were discribed first by Lord Rayleigh.

The nonlinear development of longitudinal vortices appear in the boundary layer on concave walls and reveal that the wave numbers in the streamwise direction show velocity profiles with inflection points both in the spanwise direction and normal to the wall direction[32].

According to Schmid and Henningson[27], when the disturbance achieve finite amplitude, the boundary layer flow is dominated by mushroom-type structures that can saturates and turns the flow into a new state of equilibrium, in which the secondary instabilities can grow.

The secondary instabilities that occur in Görtler vortices can be of two types: varicose and sinuous modes[26], or a medley of these. The varicose mode has its origin in the upstream region, and is related to the derivative du/dy[11]. The sinuous mode has the main feature of the fluctuation of disturbances in the xy plane, as identified in the experiment of Swearingen and Blackwelder[32].

Experimental studies[32,7,8,23], were conducted to analyze the boundary layer flow transition over concave wall providing the flow structures in the secondary instability region.

The primary flow depends only weakly int the streamwise direction. For this case Yu and Liu[34] obtained a simplified 3D instability for parallel flow and the frozen primary velocity. Yu and Liu[35] uses the energy balance in their study, to check the amplification rate from the eigenvalue problem for the parallel flow.

According to Winoto[17] the inflections are becoming larger as it develops in the downstream direction. Zhang[36] conducted an experimental study in a wind tunnel in which there was observed the development of Görtler vortices. The results showed the appearance of horseshoe type characteristic of the varicose mode of the secondary instability. They attributed the formation of these structures the shear stress in the upstream region caused by the Kelvin-Helmholtz instability.

1.1. Heat Transfer

A large amount of research has been concerned with streamwise vortices in boundary layer flows with heat transfer. Different aproaches were adopted: theoretical[25], computational[13] and experimental studies[22] on Görtler flows. The practical interest in intensifying surface heat transfer rates with the least penalty follows the need to reduce energy consumption via more efficient systems.

The Görtler vortices are responsible for generating strong distortions in the velocity profiles[13]. When the vortices amplitude is high, in the non-linear development region, a mushroom-type structure, with the streamwise velocity distribution in a crosscut plane is formed. This new velocity distribution differs from the Blasius boundary layer. Therefore, taking into account the thermal boundary layer, an spanwise–average increase in the heat transfer is observed.

Studies to explain theoretically the rate of heat transfer in a boundary layer flow over a slightly concave surface were conducted by Liu[12]. In his study it was observed that one can greatly enhance the heat transfer, paying the price of almost one to one in drag. Some experimental studies were conducted showing that the enhancement in heat transfer in Görtler flow can be higher than the one observed in turbulent flows[22].

Momayez and collaborators[21,20] conducted experiments to understand the effects of Görtler vortices and the transition to turbulence in a boundary layer with the heat transfer. They concluded that Görtler number predicts satisfactorily the different stages of Görtler stability: first primary Görtler instability appears for $Go \geq 3.5$, heat transfer reaches the turbulent level with values for $Go \geq 6.5$, the secondary instability and transition to turbulence is accomplished for $Go \geq 9$. They divided the evolution of the Stanton number in three regions: in the first region the heat transfer on the concave wall deviates gradually from the flat plate; in the second region the heat transfer coefficient gradually reaches values close to or above the turbulent boundary layer values on a flat plate; and in the third region the heat transfer ceases to increase and follows the theoretical turbulent curve. The authors say that, in the last region, the secondary instability grows rapidly and induces a premature transition to turbulence.

Other experiments were done in a similar way[33], where it was studied the development of wall shear layer stress in concave surface boundary layer flow in the presence of Görtler vortices. They analyzed the flow by hot-wire measurements, and vertical perturbation wires were adopted to introduce perturbations in a selected wavelength. The authors conclude that the spanwise-averaged wall shear stress coefficient C_f, which initially follows the Blasius curve, increases well above the local turbulent boundary layer value further downstream due to the nonlinear effects of Görtler instability and to the secondary instabilities.

The cross-sectional heat advection distribution obtained with Görtler flow is very different from the laminar boundary layer on a flat surface. According to linear theory, the boundary layer flow over a concave wall becomes unstable at some critical Görtler number[4] and its linear amplification occurs. The first effect of Görtler vortices in the wall heat transfer thus appears in its nonlinear development. Momayez[19] show that the intensification of heat transfer is related to the growth of Görtler vortices under the effect of centrifugal instability and to secondary instabilities.

In Girgis and Liu[5], the spanwise–averaged streamwise-velocity gradient, obtained by Görtler flow, is studied in terms of skin friction. The skin friction due to nonlinear steady longitudinal Görtler vortex can already nearly bridge from the local laminar skin friction to turbulent skin friction values. Their results were based in the experimental measurements[32]. The emphasis is placed on the nonlinear modification of the steady problem by Reynolds stresses of the wavy disturbance, and it is found that skin friction increases well above the turbulent boundary layer values.

The numerical study by spatial direct numerical simulation (SDNS), to analyze the heat transfer rates through the Görtler vortices without the presence of secondary instability was performed by Malatesta et al.[14]. In this study it were excited three different wavelengths in the spanwise direction 0.09, 0.18 and 0.36. Their results show that for all wavelengths it was achieved gain in the heat transfer rates.

The aim of this paper is to analyse the heat transfer rates of a flow over a concave wall, subjected first to centrifugal instability and after to secondary instability. A simulation code was developed and implemented using spatial direct numerical simulation. Disturbance were introduced for spanwise wavelenght $\lambda_z = 0.18$, free stream velocity $U_\infty =$ 3m/s, the curvature radius $R = 2$m, for Prandtl number $Pr = 0.72$. These parameters are based in the experiments carried out by Winoto and colaborators[17,18].

2. Formulation

The governing equations are the incompressible equations with constant viscosity for a Newtonian fluid. A curvilinear system was adopted, where only one remaining curvature term was maintained, and a simplified set of equations, written in vorticity-velocity formulation was adopted. Defining vorticity as the negative curl of the velocity vector and using the fact that both the velocity and the vorticity fields are solenoidal, one can obtain the following vorticity transport equation in each direction[14]:

$$\frac{\partial \omega_x}{\partial t} + \frac{\partial a}{\partial y} - \frac{\partial b}{\partial z} + \frac{Go^2}{\sqrt{Re}}\frac{\partial d}{\partial z} = \frac{1}{Re}\nabla^2\omega_x, \tag{1}$$

$$\frac{\partial \omega_y}{\partial t} + \frac{\partial c}{\partial z} - \frac{\partial a}{\partial x} = \frac{1}{Re}\nabla^2\omega_y, \tag{2}$$

$$\frac{\partial \omega_z}{\partial t} + \frac{\partial b}{\partial x} - \frac{\partial c}{\partial y} - \frac{Go^2}{\sqrt{Re}}\frac{\partial d}{\partial x} = \frac{1}{Re}\nabla^2\omega_z, \tag{3}$$

where

$$a = \omega_x v - \omega_y u, \qquad b = \omega_z u - \omega_x w, \qquad c = \omega_y w - \omega_z v, \qquad d = u^2, \tag{4}$$

are the nonlinear terms resulting from convection, vortex stretching and vortex bending. The variables (u,v, w, ω_x, ω_y, ω_z) are the velocity and vorticity components in the streamwise, wall-normal and spanwise directions respectively; t is the time. The Laplace operator is:

$$\nabla^2 = \left(\frac{\partial^2}{\partial x^2} + \frac{\partial^2}{\partial y^2} + \frac{\partial^2}{\partial z^2}\right). \tag{5}$$

The continuity equation is given by:

$$\frac{\partial u}{\partial x} + \frac{\partial v}{\partial y} + \frac{\partial w}{\partial z} = 0. \tag{6}$$

The heat transfer transport equation adopted in the present work is:

$$\frac{\partial \theta}{\partial t} + \frac{\partial u\theta}{\partial x} + \frac{\partial v\theta}{\partial y} + \frac{\partial w\theta}{\partial z} = \frac{1}{Re\ Pr}\nabla^2\theta, \tag{7}$$

where θ is the non dimensional temperature given by $\theta = (T - T_0)/(T_\infty - T_0)$, where T is the dimensional temperature, and T_∞ and T_0 are the temperature values outside from the thermal boundary layer and at the wall, respectively.

3. Numerical Method

The flow is assumed to be periodic in the spanwise direction. Therefore, the flow field can be expanded in Fourier series with K spanwise Fourier modes:

$$\psi(x, y, z, t) = \sum_{k=0}^{K} \Psi_k(x, y, t) e^{(i\beta_k z)}, \tag{8}$$

where

$\psi = u, v, w, \omega_x, \omega_y, \omega_z, \theta, a, b, c, d, e, f, g$;

and

$\Psi_k = U_k, V_k, W_k, \Omega_{x_k}, \Omega_{y_k}, \Omega_{z_k}, \Theta_{z_k}, A_k, B_k, C_k, D_k, E_k, F_k, G_k$;

and β_k is the spanwise wavenumber given by $\beta_k = 2\pi k/\lambda_z$, and λ_z is the spanwise wavelength of the fundamental spanwise Fourier mode, and $i = \sqrt{-1}$. The number of modes adopted in the simulations carried out here was $K = 21$ with 64 points in the physical space. A higher number of modes was tested, but the results did not change, which shows that the adopted value was enough for the steady simulations.

The governing equations in the Fourier space:

$$\frac{\partial \Omega_{x_k}}{\partial t} + \frac{\partial A_k}{\partial y} - \beta_k B_k - \frac{Go^2}{\sqrt{Re}}\beta_k(D_k^2) = \frac{1}{Re}\nabla_k^2 \Omega_{x_k}, \tag{9}$$

$$\frac{\partial \Omega_{y_k}}{\partial t} + \beta_k C_k - \frac{\partial A_k}{\partial x} = \frac{1}{Re}\nabla_k^2 \Omega_{y_k}, \tag{10}$$

$$\frac{\partial \Omega_{z_k}}{\partial t} + \frac{\partial B_k}{\partial x} + \frac{\partial C_k}{\partial y} - \frac{Go^2}{\sqrt{Re}}\frac{\partial (D_k^2)}{\partial x} = \frac{1}{Re}\nabla_k^2 \Omega_{z_k}, \tag{11}$$

$$\frac{\partial^2 U_k}{\partial x^2} - \beta_k^2 U_k = -\beta_k \Omega_{y_k} - \frac{\partial^2 V_k}{\partial x \partial y}, \tag{12}$$

$$\frac{\partial^2 V_k}{\partial x^2} + \frac{\partial^2 V_k}{\partial y^2} - \beta_k^2 V_k = -\frac{\partial \Omega_{z_k}}{\partial x} + \beta_k \Omega_{x_k}, \tag{13}$$

$$\frac{\partial^2 W_k}{\partial x^2} - \beta_k^2 W_k = \frac{\partial \Omega_{y_k}}{\partial x} + \beta_k \frac{\partial V_k}{\partial y}, \tag{14}$$

$$\frac{\partial \Theta_k}{\partial t} + \frac{\partial E_k}{\partial x} + \frac{\partial F_k}{\partial y} - i\beta_k G = \frac{1}{Re\, Pr}\nabla_k^2 \Theta_k, \tag{15}$$

where $\nabla_k^2 = \left(\frac{\partial^2}{\partial x^2} + \frac{\partial^2}{\partial y^2} - \beta_k^2\right)$.

The time derivatives in the vorticity transport equations were discretized with a classical fourth-order Runge-Kutta integration scheme[3]. The spatial derivatives were calculated using a sixth-order compact finite difference scheme[10,28,30]. The V-Poisson equation was solved using a multigrid full approximation scheme[31]. A V-cycle scheme working with four grids was implemented.

3.1. Boundary Conditions

The governing equations are complemented by the specification of boundary conditions. At the wall ($y = 0$), a non-slip condition was imposed for the streamwise (U_k) and the spanwise (W_k) velocity components. The wall normal velocity component (V_k) was specified at the suction and blowing strip region between x_1 and x_2 , where the disturbances were introduced. Away from the disturbance generator, this velocity component was set to zero. The function used for the wall-normal velocity $V_k = 1$ at the disturbance generator is:

$$V_{k=1}(i, 0, t) = A \sin^3(\epsilon) \quad \text{for} \quad x_1 \le i \le x_2 \quad \text{and}$$

$$V_{k=1}(i, 0, t) = 0 \quad \text{for} \quad x < x_1 \quad \text{and} \quad x > x_2, \tag{16}$$

where $\epsilon = (x - x_1)/(x_2 - x_1)$ and A is a real constant chosen to adjust the amplitude of the disturbance. For all modes $k \neq 1$ the value of $V_k = 0$ at the wall was settled.

At the inflow boundary ($x = x_0$), the velocity, vorticity components, and temperature are specified based on the similarity solutions. At the outflow boundary ($x = x_{max}$), the second derivatives with respect to the streamwise direction of the velocity and vorticity components are set to zero. At the upper boundary ($y = y_{max}$), the flow is considered non-rotational. This is satisfied by setting all vorticity components and their derivatives to zero. The wall-normal velocity component at the upper boundary was settled according to the following condition:

$$\left.\frac{\partial V_k}{\partial y}\right|_{x, y_{max}, t} = 0. \tag{17}$$

This condition was imposed in the solution of the U_k velocity in the Poisson equation. The equations used for evaluating the vorticity components at the wall are:

$$\frac{\partial^2 \Omega_{x_k}}{\partial x^2} - \beta_k^2 \Omega_{x_k} = -\frac{\partial^2 \Omega_{y_k}}{\partial x \partial y} - \beta_k \nabla_k^2 V_k \tag{18}$$

$$\frac{\partial \Omega_{z_k}}{\partial x} = \beta_k \Omega_{x_k} - \nabla_k^2 V_k. \tag{19}$$

A damping zone near the outflow boundary was defined in which all the disturbances are gradually damped down to zero[9]. This technique is used to avoid reflections in the outflow boundary. Meitz[16] adopted a fifth order polynomial, and the same function was used in the present code. The basic idea is to multiply the vorticity components by a ramp function $f_1(x)$ after each sub-step of the integration method. Using this technique, the vorticity components are taken as:

$$\Omega_k(x, y, t) = f_1(x)\Omega_k^*(x, y, t), \tag{20}$$

where $\Omega_k^*(x, y, t)$ is the disturbance vorticity component that results from the Runge-Kutta integration and $f_1(x)$ is a ramp function that goes smoothly from 1 to 0. The implemented function was:

$$f_1(x) = f(\epsilon) = 1 - 6\epsilon^5 + 15\epsilon^4 - 10\epsilon^3, \tag{21}$$

where $\epsilon = (x - x_3)/(x_4 - x_3)$ for $x_3 \leq x \leq x_4$. To ensure good numerical results, a minimum distance between x_3 and x_4 and between x_4 and the end of the domain, x_{max} has to be adopted[9]. In the simulations presented here, each zone had 30 grid points.

Another buffer domain located near the inflow boundary was also implemented in the code. As pointed out by Meitz[15], in simulations involving streamwise vortices, reflections due to the vortices at the inflow can contaminate the numerical solution. The damping function is similar to the one used for the outflow boundary.

$$f_2(x) = f(\epsilon) = 6\epsilon^5 - 15\epsilon^4 + 10\epsilon^3, \tag{22}$$

where $\epsilon = (x - 1)/(x_1 - 1)$ for the range $1 \leq x \leq x_1$. All the vorticity components were multiplied by this function in this region. The boundary conditions for the temperature were:

- inflow – $\theta = 0$;
- outflow – $\theta = 0$, since the same buffer domain for the vorticity was also applied for the temperature;
- wall – $\theta = 0$;
- upper boundary – the values were obtained from the heat transfer transport equation.

The method and code adopted in the present paper has been validated and verified for the hydrodynamic boundary layer[29].

4. Results

In the validation test case the parameters used were those of the experiment of[17,18]. They considered a boundary layer on a concave plate with $\bar{R} = 2$ m and free-stream velocity $\bar{U}_\infty = 3$ m/s. The numerical domain starts at $x_0 = 200$ mm downstream the leading edge which corresponds to a Reynolds number $Re = 33124$. In the experiment, the average spanwise wavelength was $\bar{\lambda}_z = 15$ mm, which corresponds to a non-dimensional wavenumber of $\beta = 83.78$. The reference length used is $\bar{L} = 0.2$ m. The number of grid points used was 1177 and 201 in the streamwise and the wall-normal directions, respectively. The non-dimensional uniform grid spacing is 3.5×10^{-3} and 4.0×10^{-4} in the streamwise and the wall-normal directions, respectively. The disturbance-strip location for the stationary disturbances introduction was $4.035 \times 10^{-4} \leq Re_x \leq 4.505 \times 10^{-4}$. 21 Fourier modes were used in the simulation. Test runs with a smaller grid spacing and larger number of Fourier modes indicated that the solutions were grid independent.

Figure 1 shows the maximum amplitude of the streamwise disturbance velocity u of each frequency over (z, y) plane in the streamwise direction $Re_x = \frac{U_\infty x}{\nu} = \frac{3.0 \quad x}{1.5651\times10^{-5}}$. The unsteady frequencies introduced range from 18.75 Hz to 300 Hz in steps of 18.75 Hz. These disturbances were introduced via suction and blowing at the wall in 3 different streamwise positions $Re_x \sim 7.5 \times 10^4$, $Re_x \sim 9.5 \times 10^4$ and $Re_x \sim 1.15 \times 10^5$. Initially all the forced modes exhibit a stable behavior until the streamwise position of $Re_x \sim 1.25 \times 10^5$, where all modes grow due to the onset of secondary instability. The frequencies with the higher values of growth rates in the secondary instability region are 18.75, 112.50, 130.25 and 141.00 Hz – these frequencies are highlighted in the figure.

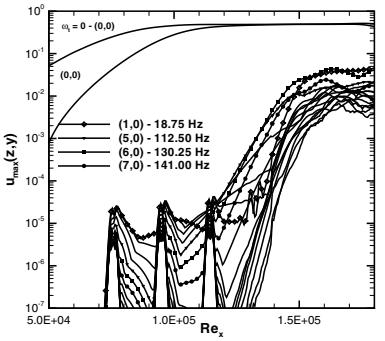

Fig. 1. Maximum amplitude of the disturbance streamwise velocity u of each frequency over (z, y) plane in the streamwise direction Re_x

The temperature distribution over $z \times y$ slices and the structures obtained in the simulation and the Q isosurfaces are shown in the Fig. 4 at two time instances. The flow is from bottom left to top right. The mushroom structure formed by the thermal boundary layer can be observed in the $z \times y$ slices. The Q isosurfaces show initially the steady Görtler vortices. After a certain streamwise position the secondary instabilities appear and the dominant structures are typical for a varicose mode.

Fig. 2. Isosurfaces obtained with $Q = 0.5$ colored by temperature (θ) and the temperature distribution over a $z \times y$ slices.

The streamwise evolution of the spanwise–and–time–average Stanton number is shown in Fig. 3. At the beginning when the vortices are in the linear development region and the Stanton curve is on top of the laminar curve. In the nonlinear region, after $Re_x \sim 1.05 \times 10^5$ the Görtler vortices intensify the heat transfer reaching higher values than the turbulent curve. Downstream of $Re_x \sim 1.7 \times 10^5$ all the modes have high amplitudes, close to the turbulent region, and this phenomena decreases the spanwise–and–time average heat transfer rate.

5. Conclusion

In the present paper it was analysed the centrifugal instability mechanism and secondary instabilities in a boundary layer flow over concave wall. The parameters adopted for the simulations were based in the experiment of Winoto

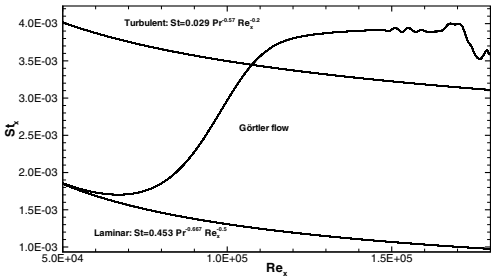

Fig. 3. Streamwise evolution of the spanwise–and–timeaverage Stanton number.

and collaborators[17,18] and the Prandtl number adopted was $Pr = 0.72$. The results showed that the primary instability (Görtler vortices) increases the heat transfer rate to values above the turbulent values in the nonlinear development region. It was introduced non stationary disturbances to seed secondary instabilities. These disturbances were introduced to induce the varicose mode, since this kind of mode was observed experimentally. The spanwise–and–time average Stanton number analysis showed that this secondary instability keeps the heat transfer with high values only in a short region and this value should decay to turbulent value downstream.

6. Acknowledgements

The authors acknowledge the financial support received from FAPESP under Grant No. 2010/00495-1.

References

1. M. Clauser and F. Clauser. The effect of curvature on the transition from laminar to turbulent boundary layer. technical report naca tn-163. *National Advisory Commite of Aeronautics*, 1937.
2. P. G. Drazin and W. H. Reid. *Hydrodynamic Stability*. Cambridge University Press, 2004.
3. J. H. Ferziger and M. Peric. *Computational Methods for Fluid Dynamics*. Springer-Verlag Berlin Heidelberg New York, 1997.
4. J. M. Floryan and W. S. Saric. Stability of Görtler vortices in boundary layers. *AIAA Journal*, 20:316–324, 1982.
5. I. G. Girgis and J. T. C. Liu. Nonlinear mechanics of wavy instability of steady longitudinal vortices and its effect on skin friction rise in boundary layer flow. *Physics of Fluids*, 18, 2006.
6. H. Goerlter. On the three dimensional instability of laminar boundary layer on concave walls. technical report naca tm-1375. *National Advisory Commite of Aeronautics*, 1940.
7. K. Inagaki and Y. Aihara. An experimental study of the transition region of the boundary-layer along a concave wall. *European Journal of Mechanics - B/Fluids*, 14:143–168, 1995.
8. A. Ito. Breakdown structure of longitudinal vortices along a concave wall. *Journal of Japan Society for Aeronautical and Space Sciences*, 166-173:33, 1985.
9. M. Kloker, U. Konselmann, and H.F. Fasel. Outflow boundary conditions for spatial navier-stokes simulations of transition boundary layer. *AIAA Journal*, 31:620–628, 1993.
10. S. K. Lele. Compact finite difference schemes with spectral-like resolution. *Journal of Computational Physics*, 103:16–42, 1992.
11. F. Li and M. R. Malik. Fundamental and subharmonic secondary instabilities of grtler vortices. *Journal of Fluid Mechanics*, 297:77–100, 1995.
12. J. T. C. Liu. Nonlinear instability of developing streamwise vortices with applications to boundary layer heat transfer intensification thought an extended reynolds analogy. *Philosophical Transactions of the Royal Society*, 366:101–112, 2008.
13. J. T. C. Liu and K. Lee. Heat transfer in a strongly nonlinear spatially developing longitudinal vorticity system. *Physics of Fluids*, 7:559–599, 1995.
14. V. Malatesta, L. F. S. Souza, and J. T. C. Liu. Influence of goertler vortices spanwise wavelength on the heat transfer rates. *Computational Thermal Sciences*, 5:389–400, 2013.
15. H. L. Meitz. *Numerical Investigation of Suction in a Trasition Flat-Plate Boundary Layer*. PhD thesis, The University of Arizona, 1996.
16. H.L. Meitz and H.F. Fasel. A compact-difference scheme for the navier-stokes equations in vorticity-velocity formulation. *Journal of Computational Physics*, 157:371–403, 2000.
17. H. Mitsudharmadi, S. H. Winoto, and D. A. Shah. Development of boundary-layer flow in the presence of forced wavelength goertler vortices. *Physics of Fluids*, 16, 2004.
18. H. Mitsudharmadi, S. H. Winoto, and D. A. Shah. Splitting and merging of Görtler vortices. *Physics of Fluids*, 17(12):1–12, 2005.
19. L. Momayez, P. Dupont, G. Delacourt, O. Lottin, and H. Peershossaini. Genetic algorithm based correlations for heat transfer calculation on concave surfaces. *Applied Thermal Engineering*, 29:3476–3481, 2009.

20. L. Momayez, P. Dupont, and H. Peershossaini. Effects of vortex organization on heat transfer enhancement by goertler instability. *International Journal of Thermal Sciences*, 43:753–760, 2004.
21. L. Momayez and H. Peershossaini. Some unexpected effects of wavelenght and pertubation strength on heat transfer enhancement by Görtler instability. *International Journal of Heat and Mass Transfer*, 47:495–492, 2004.
22. H. Peerhossaini. *L'Instabilite d'une couche limite sur une paroi concave (les tourbilons de Görtler.* PhD thesis, Univ. Pierre et Marie Curie, Paris, 1987.
23. H. Peerhossaini and J. E. Wesfreid. On the inner structure of streamwise gortler rolls. *International Journal of Heat and Fluid Flow*, 12:9, 1988.
24. L. Rayleigh. On the dynamics of revolving fluids. *Philosophical Transactions of the Royal Society*, 93:148–154, 1917.
25. P. G. Saffmann. *Vortex Dynamics*. Cambridge University Press, 1992.
26. W. S. Saric. Görtler vortices. *Annu. Rev. Fluid Mech.*, 26:379–409, 1994.
27. P. J. Schmid and D. S. Henningson. *Stability and Transition in Shear Flows*, volume 142. Springer, New York, 2001.
28. L. F. Souza. *Instabilidade Centrífuga e Transição para Turbulência em Escoamentos Laminares sobre Superfícies Côncavas*. PhD thesis, Instituto Tecnológico de Aeronáutica, Brazil, 2003.
29. L. F. Souza, M. T. Mendona, M. A. F. de Medeiros, and M. Kloker. Seeding of goertler vortices through a suction and blowing strip. *Journal of the Brazilian Society of Mechanical Sciences*, 26:269–279, 2004.
30. L. F. Souza, M. T. Mendonça, and M. A. F. Medeiros. The advantages of using high-order finite differences schemes in laminar-turbulent transition studies. *International Journal for Numerical Methods in Fluids*, 48:565–592, 2005.
31. K. Stuben and U. Trottenberg. *Nonlinear Multigrid Methods, the Full Approximation Scheme*. Koln-Porz, 1981.
32. J.D. Swearingen and R.F. Blackwelder. The growth and breakdown of streamwise vortices in the presence of a wall. *Journal of Fluid Mechanics*, 182:255–290, 1987.
33. Tandiono, S. H. Winoto, and D. A. Shah. Wall shear stress in goertler sortex boundary layer flow. *Physics of Fluids*, 21, 2009.
34. X. Yu and J. T. C. Liu. The secondary instability in goertler flow. *Physics of Fluids*, 3:1845–1847, 1991.
35. X. Yu and J. T. C. Liu. On the mechanism of sinuous and varicose modes in threedimensional viscous secondary instability of nonlinear grtler rolls. *Physics of Fluids*, 6:736–750, 1994.
36. D. H. Zhang, S. H. Winoto, and Y. T. Chew. Measurement in laminar and transitional boundary-layer flows on concave surface. *International Journal of Heat and Fluid Flow*, 16:88–98, 1995.